

Geophysical Research Letters

RESEARCH LETTER

10.1029/2021GL094282

Special Section:

Probing the Magnetosphere through Magnetoseismology and Ultra-Low-Frequency Waves

Key Points:

- 2D spatial structures and time evolution of high-m ultralow frequency (ULF) waves are revealed for the first time using total electron content (TEC) data
- ULF waves in TEC data show high coherence, similar temporal distribution and frequency evolution with wave signatures in GOES *B_x* data
- The high-m waves caused neither ionospheric scintillations nor ground magnetic signatures

Supporting Information:

Supporting Information may be found in the online version of this article.

Correspondence to:

X. Shi,
xueling7@vt.edu

Citation:

Zhai, C., Shi, X., Wang, W., Hartinger, M. D., Yao, Y., Peng, W., et al. (2021). Characterization of high-m ULF wave signatures in GPS TEC data. *Geophysical Research Letters*, *48*, e2021GL094282. <https://doi.org/10.1029/2021GL094282>

Received 10 MAY 2021

Accepted 25 JUN 2021

Characterization of High-m ULF Wave Signatures in GPS TEC Data

Changzhi Zhai¹ , Xueling Shi^{2,3} , Wenbin Wang³ , Michael D. Hartinger⁴ , Yibin Yao⁵ , Wenjie Peng⁵, Dong Lin³ , J. Michael Ruohoniemi² , and Joseph B. H. Baker² 

¹School of Earth Sciences and Engineering, Hohai University, Nanjing, Jiangsu, China, ²Department of Electrical and Computer Engineering, Virginia Tech, Blacksburg, VA, USA, ³High Altitude Observatory, National Center for Atmospheric Research, Boulder, CO, USA, ⁴Space Science Institute, Boulder, CO, USA, ⁵School of Geodesy and Geomatics, Wuhan University, Wuhan, Hubei, China

Abstract GPS total electron content (TEC) measurements were used to investigate high-m ultralow frequency (ULF) waves during the recovery phase of a geomagnetic storm. ULF wave signals in TEC data show high coherence and significant common power in the wavelet coherence and cross wavelet transform analyses with magnetic field radial component data from GOES-15. They did not cause significant ionospheric scintillation or ground magnetic signatures due to ionospheric screening effects. An automatic identification procedure is developed to identify ULF wave signature in TEC data from 10 GPS receivers on January 25, 2016. The waves were mainly distributed on the dayside and post dusk sector from $\sim 64^\circ$ to $\sim 71^\circ$ magnetic latitude. This is the first time that the large-scale 2D spatial structure and temporal evolution of high-m ULF waves are revealed, which demonstrates TEC measurements as an effective high-m ULF wave remote sensing tool.

Plain Language Summary Ultralow frequency (ULF) waves with periods from 1 s to more than 10 min can interact with particles in the magnetosphere and affect the ionospheric electric field as well as the geomagnetic field. Determining how ULF waves propagate from the magnetosphere to the ionosphere, and ground, and how the wave power is distributed spatially and evolves over time is important for understanding the role of ULF waves in magnetosphere-ionosphere coupling. ULF waves with large azimuthal wave numbers (high-m) are usually screened from the ground by the ionosphere and thus not detected by magnetometers. Due to the limitations in spatial coverage of satellites and ground radar observations, it has been difficult to examine the large-scale spatial structure and temporal evolution of high-m ULF waves during a single event. In this study, we used data from multiple instruments to analyze the characteristics of the high-m ULF waves that occurred during January 24–26, 2016. The ULF wave signatures in GPS total electron content (TEC) showed similar time evolution and frequency variations to GOES satellite measurements. By using abundant GPS TEC data and automatic identification procedure, the large-scale 2D spatial structure and time evolution of high-m ULF waves are disclosed for the first time.

1. Introduction

Ultralow frequency (ULF) waves cover the frequency range from 1 mHz to about 1 Hz. They can be classified into two types: pulsations continuous (Pc) and pulsations irregular (Pi) according to their waveform and wave period (Jacobs et al., 1964). Alfvén waves with radial and azimuthal magnetic field oscillations are known as poloidal and toroidal ULF waves, respectively. Poloidal waves with azimuthal electric fields have been extensively studied since they can have strong wave-particle resonant interactions with unstable particle populations and influence the dynamics of the inner magnetosphere (Baddeley et al., 2004; Le et al., 2017; Zong et al., 2009). Observations from various satellite missions (e.g., Van Allen Probe, THEMIS, Cluster) have been used to investigate ULF wave propagation in the magnetosphere and to estimate their azimuthal wave numbers (*m* values) (e.g., Shah et al., 2016; Takahashi et al., 2018; Zong et al., 2007). Ground-based measurements from the Super Dual Auroral Radar Network (SuperDARN) high frequency radars (Shi, Baker, et al., 2018) and magnetometers (Ren et al., 2015; Sarris et al., 2009) have also been used to analyze the local time distribution of ULF waves in the ionosphere.

Ionospheric total electron content (TEC) data has been used to study ULF waves in the ionosphere for decades. Davies and Hartmann (1976) found small ($<0.1\%$) TEC fluctuations during magnetically quiet days which were associated with micropulsations observed on the ground and in the magnetosphere. Skone (2009) analyzed the statistical relationship between Pc3 pulsations and GPS Vertical TEC (VTEC) variations and found that the variations of magnetic Pc3 pulsations and ionospheric VTEC variations are similar. Watson et al. (2015, 2016) reported TEC variations related to Pc4 and Pc5-6 ULF waves, with the Pc5-6 waves showing large peak-to-peak amplitudes of 2–7 TECU. In addition to VTEC fluctuations, the ionospheric scintillations are also found to be related to Pc1 and Pc5 pulsations (Francia et al., 2020; Yizengaw et al., 2018). Previous studies have shown that the TEC technique is sensitive enough to detect ionospheric response to ULF waves.

Due to the ionospheric screening effects (Hughes & Southwood, 1976) and radar sampling biases (Shi, Ruohoniemi, et al., 2018), high-m ULF waves are difficult to detect on the ground. In-situ space-based measurements are sparse and often inadequate for obtaining wave spatial distributions. Taking advantage of widely distributed GPS receivers, TEC observations can provide a great opportunity to investigate the spatial distribution, propagation, and time evolution of high-m ULF waves. Coordinated geophysical measurements from GOES, SuperDARN, GPS and ground magnetometers are used in this study to examine high-m ULF wave properties. Using VTEC measurements from 10 GPS receivers, we analyze the temporal evolution and 2D spatial structure of ULF waves in the ionosphere.

2. Event Overview and Methodology

High-m ULF waves were observed on January 24–26, 2016 during the recovery phase of a moderate geomagnetic storm (minimum Dst = -95 nT, Figure 1a). An overview of the event and the instrument locations is presented in Figure 1. A substorm indicated by the AE index enhancement occurred on January 24, 2016 from 18 to 20 UT (Figure 1b). The substorm onset was associated with a southward excursion of the IMF Bz component (Figure 1c) at ~ 18 UT. The AE index peaked at a maximum value of $\sim 1,000$ nT at $\sim 19:00$ UT followed by a solar wind dynamic pressure enhancement that peaked at $\sim 20:00$ UT (Figure 1d). Figure 1e shows the distribution of multi-instruments in the altitude-adjusted corrected geomagnetic coordinates (Shepherd, 2014) at 00:00 UT on January 25, 2016. Note that the GPS receiver FSIC, the ground magnetometer FSIM, and the PGR radar are close to the footprint of GOES-15.

TEC data used in this study are derived from 1 Hz GPS carrier phase observations. Slant TEC was converted to vertical TEC based on the zenith angle of GPS signals at their pierce points. The cut off angle is 25° and the altitude of ionospheric pierce points (IPP) is 450 km. GPS satellites are identified by their pseudo random noise (PRN) number. The magnetic field data from GOES-13 and GOES-15 are sampled at 0.512 s and are expressed in local mean-field-aligned (MFA) coordinates. The mean magnetic field data are obtained by a 30-minute running average. The three magnetic components in MFA coordinates are B_r (outward, perpendicular to the mean magnetic field), B_ϕ (eastward, perpendicular to the mean magnetic field), and B_\parallel (parallel to the mean magnetic field). Magnetic perturbations in the B_\parallel direction (ΔB_\parallel) are derived by subtracting the 30-minute averaged mean magnetic field. Thus, the signal components below 0.55 mHz are filtered out. Line-of-sight (LOS) plasma velocity observations from the SuperDARN Prince George (PGR) radar are used to detect the ionospheric response to the ULF waves. Ground magnetic field data with 2 Hz sampling rate are also detrended by subtracting a 30-minute running average. A continuous wavelet transform (CWT) (Foufoula-Georgiou and Kumar, 2014) is used to obtain the power spectral density (PSD) of the various data sets. wavelet coherence (WTC) and cross wavelet transform (XWT) (Grinsted et al., 2004) are used to examine the correlation between the ULF signals in the GOES and GPS VTEC measurements.

3. Results

3.1. ULF Wave Observations From Space to the Ground

As shown in Figure 1e, the FSIC GPS receiver, SuperDARN PGR radar camping beam, and FSIM ground magnetometer are all located close to the GOES-15 footprint. We take advantage of this to validate the ULF wave signatures in GPS VTEC and to investigate the different responses of the magnetosphere, ionosphere and geomagnetic field to high-m ULF waves. Figure 2 shows the time series and PSD from various space-

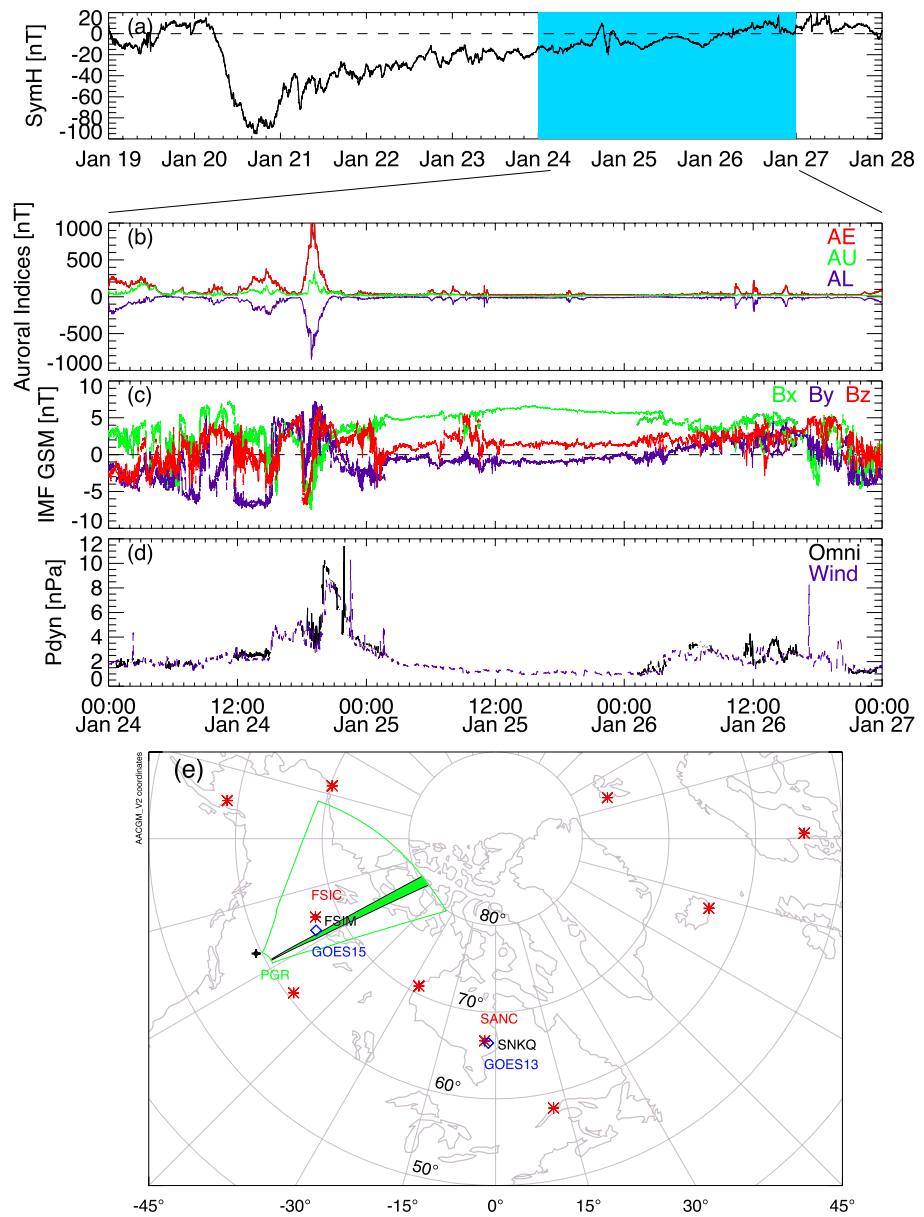


Figure 1. Geomagnetic indices, interplanetary parameters and instrumentation used in this study. (a) SymH index during January 19–27, 2016, the cyan-shaded region identifies the time interval of high-m wave occurrence; (b) AE (red), AU (green) and AL (purple) indices; (c) Bx (green), By (purple) and Bz (red) components of interplanetary magnetic field in GSM coordinates; (d) OMNI (black) and Wind (purple) solar wind dynamic pressure during January 24–26, 2016; (e) GPS stations (red asterisks), footprints of GOES 13 and 15 (blue diamonds), ground magnetometers (black dots), field-of-view of the Super Dual Auroral Radar Network Prince George radar (green fan), camping beam with 6 s high-time resolution measurements (green shaded region) in altitude-adjusted corrected geomagnetic coordinates at 00:00 UT on January 25, 2016.

and ground-based instruments. As seen from Figure 2a, sinusoidal waveforms appeared in B_{ϕ} and B_r (larger amplitude in the mode) during the period 22:15–24:00 UT. Figure 2b shows the dominant frequency of the monochromatic signal in B_r is ~ 10 mHz. The time series and PSD of SuperDARN PGR radar observations also showed similar wave signatures at the same frequency (Figures 2c and 2d).

FSIC PRN 03 and PRN 23 detrended VTEC obtained by subtracting 10-minute running average are shown in Figure 2e. Although there are low frequency variations, the superposed high-frequency monochromatic sinusoidal waveforms are still evident. For visualization purposes, VTEC signals are filtered with a third

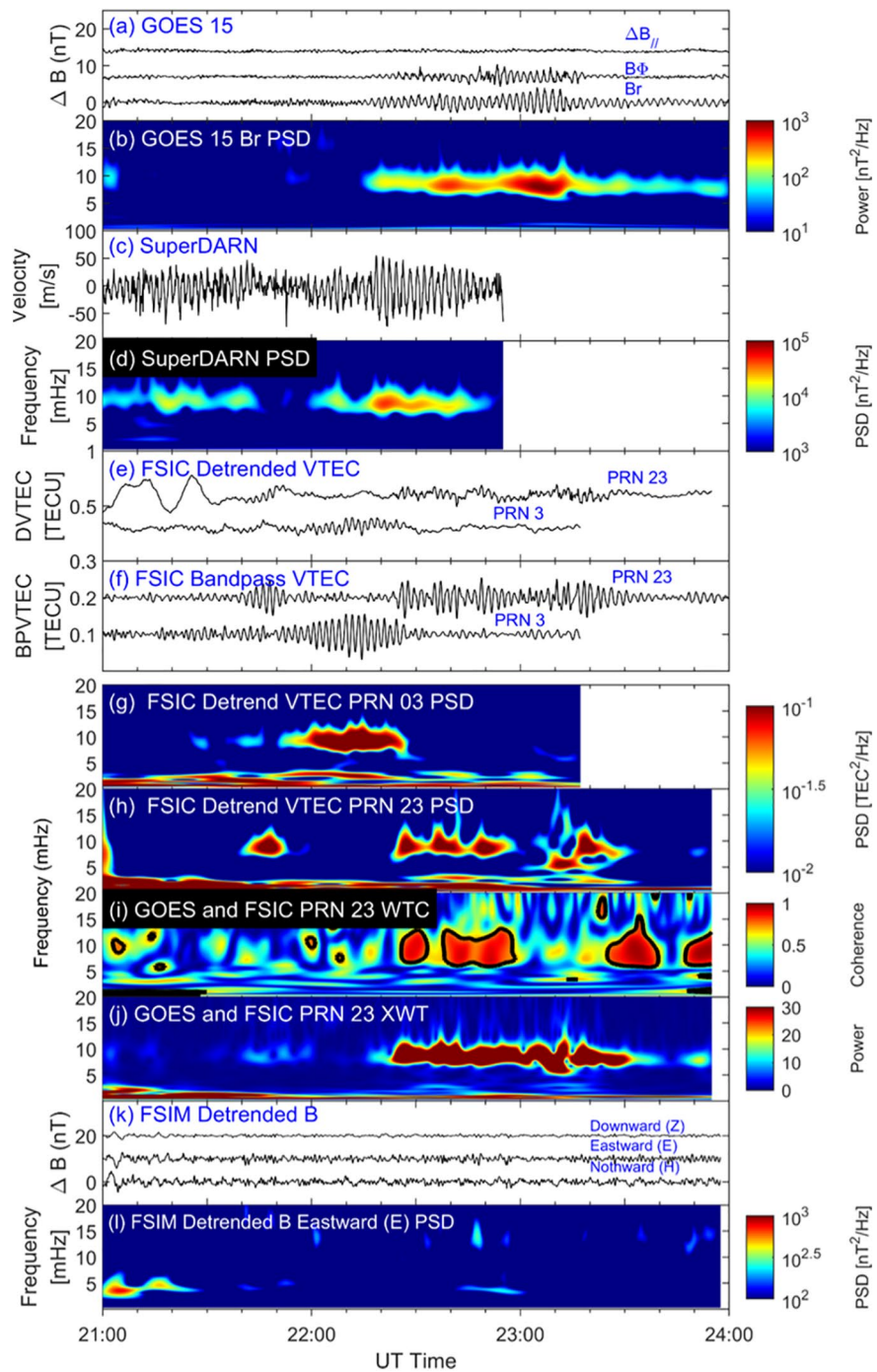


Figure 2. Time series and power spectral density (PSD) stack-plot of ground- and space-based observations of high-m ultralow frequency wave activity between 21:00 and 24:00 UT on January 25, 2016. (a) Time series of GOES-15 magnetic field data in the mean-field-aligned coordinate system, (b) PSD of the GOES-15 B_{\parallel} component; (c–d) time series and PSD of Super Dual Auroral Radar Network Prince George radar beam 12 gate 9 LOS velocity; (e–f) detrended and bandpass GPS vertical TEC (VTEC) data observed at the FSIC magnetometer; (g–h) PSDs of pseudo random noise (PRN) 03 and PRN 23 detrended VTEC; (i–j) wavelet coherence and cross wavelet transform of the GOES-15 B_{\parallel} component and FSIC PRN 23 detrended VTEC; (k) time series of magnetic field perturbations observed at the FSIM station; (l) PSD of the FSIM magnetic field eastward perturbations.

order Butterworth bandpass filter (5–20 mHz) and shown in Figure 2f. VTEC disturbances with 0.1 TECU peak-to-peak amplitudes were registered in both PRN 03 and PRN 23. Figures 2g and 2h display the PSDs of PRN 03 and PRN 23 detrended VTEC. Significant narrowband power around 10 mHz can be seen during 21:50–22:40 UT in the PRN 03 data and during 21:40–23:00 UT in the PRN 23 data. High-m waves are usually localized in L-shell. Depending on the orbit of GOES-15 and GPS satellites, the ULF waves observed by GOES-15 and GPS receivers were sporadic. The time delay in the appearance of the narrowband waves in FSIC VTEC (Figures 2g and 2h) and those in GOES-15 observations (Figures 2a and 2b) is attributed to waves observed at different regions rather than the same wave packet propagated from one location to another. Figures 2i and 2j give the WTC and XWT results of GOES-15 B_r and PRN 23 detrended TEC. The 5% significance level against the red noise is shown as thick contours in Figure 2i. High coherence and significant common power during the time period of 22:20–23:00 UT suggest that FSIC PRN 23 observed the same ULF waves as GOES-15.

Figure 2k shows perturbations in the geographic downward (Z), eastward (E), and northward (N) components of the magnetic field observed at the FSIM station. No sinusoidal signatures appeared in the three FSIM magnetic perturbations and the PSD of the FSIM eastward (poloidal component) did not show any of the narrowband power around 10 mHz seen in the GOES B_r (Figure 2b) and VTEC data (Figures 2g and 2h). This indicates that the high-m poloidal wave signals observed by the GOES satellite, SuperDARN radar and FSIC receiver were high-m mode and thus not observed by the FSIM ground magnetometer because they were screened by the ionosphere.

3.2. ULF Wave Distribution and Relationship With Ionospheric Scintillation

Figures 2i and 2j has shown that the detrended VTEC data has high coherence and significant common power with the high-m ULF wave signatures seen in the GOES B_r data. We now further investigate the magnetic latitude (MLAT) and universal time (UT) distribution of these ULF waves by examining the WTC and XWT results of GOES-15 B_r and VTEC data at FSIC using 32 separate GPS satellites. The peak power of XWT results below 20 mHz and corresponding WTC results are filtered by $WTC > 0.7$ and $XWT > 15$ (see Text S1 and Figure S1 in Supporting Information for details). The results are provided in Figure 3 which shows the high-m ULF wave distribution in GOES-15 B_r and GPS TEC from January 24 to January 26 in 2016 and their relationship with ionospheric scintillation. Figure 3a gives the PSD below 20 mHz from the GOES-15 B_r data. The distributions of the filtered wave signatures according to the stated criteria are shown in Figures 3b–3d. In Figures 3b–3e, the red (black) vertical lines indicate local noon (midnight) time, the green (blue) vertical lines indicate local dawn (dusk) time.

Panel 3a shows ~10 mHz ULF waves were observed from local noon to dusk on January 24 and monochromatic ULF waves were observed across the dayside on January 25 and 26. The wave frequency decreased from around 10 mHz for the first time GOES-15 passed through the wave active region to around 6 mHz during the third pass. The WTC (Figure 3b) and XWT (Figure 3c) analyses of the FSIC TEC data and GOES-15 B_r data show that the ULF wave signatures in TEC data have high coherence and significant common power with those observed by GOES-15. The ULF wave signatures are primarily distributed between ~62° and ~68° MLAT on the dayside. Figure 3d shows the frequency distribution color-coded as a function of MLAT and UT. Similar frequency-time evolution of the waves can be seen in the GOES-15 B_r and VTEC data, that is, both have a general decreasing trend with time. Similar WTC and XWT analyses applied to the TEC data from the SANC GPS receiver and GOES-13 B_r data (see Figure 1e for locations) produced similar results (not shown).

Besides analyzing the MLAT and UT time distribution of high-m ULF waves in GPS VTEC, we also checked the correlation between the waves and ionospheric scintillation using the phase sigma (the standard deviation of the detrended carrier phase) and S4 (standard deviation of the received signal power normalized to average signal power) indices. Figure 3e shows the phase sigma index MLAT versus UT distribution while Figure 3f shows the phase sigma value versus the elevation angle distribution. The mean values of selected phase sigma and all phase sigma are 0.0165 and 0.0182 rad, respectively, and median values of the two data sets are 0.170 and 0.180 rad, respectively. This suggests the high-m ULF waves during this particular event had little contribution to ionospheric phase scintillation. We also checked the S4 index (not shown), and

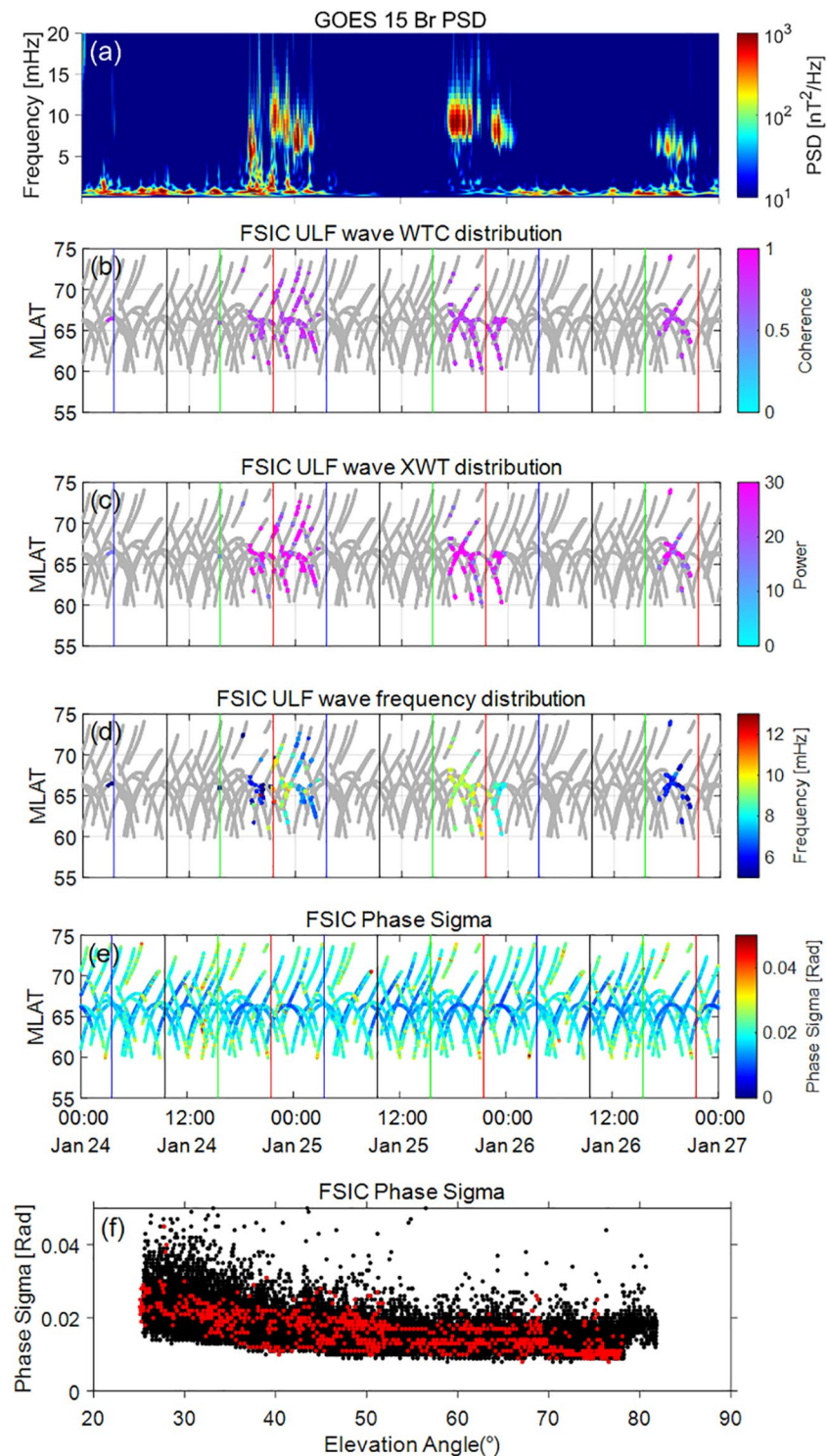


Figure 3. High-m ultralow frequency (ULF) wave distribution in GOES-15 B_r and GPS total electron content (TEC) from January 24 to January 26 in 2016 and their relationship with ionospheric scintillation. (a) PSD of GOES-15 B_r ; (b)–(c) the distribution of filtered WTC and XWT between the FSIC detrended vertical TEC (VTEC) and the GOES-15 B_r component; (d) the distribution of selected ULF wave frequency in FSIC VTEC; (e) phase sigma index distribution of FSIC; (f) phase sigma versus elevation angle distribution of all data records (black dots) and ULF wave related data records (red dots). Gray lines in panels (b)–(d) indicate the distribution of all the GPS VTEC data.

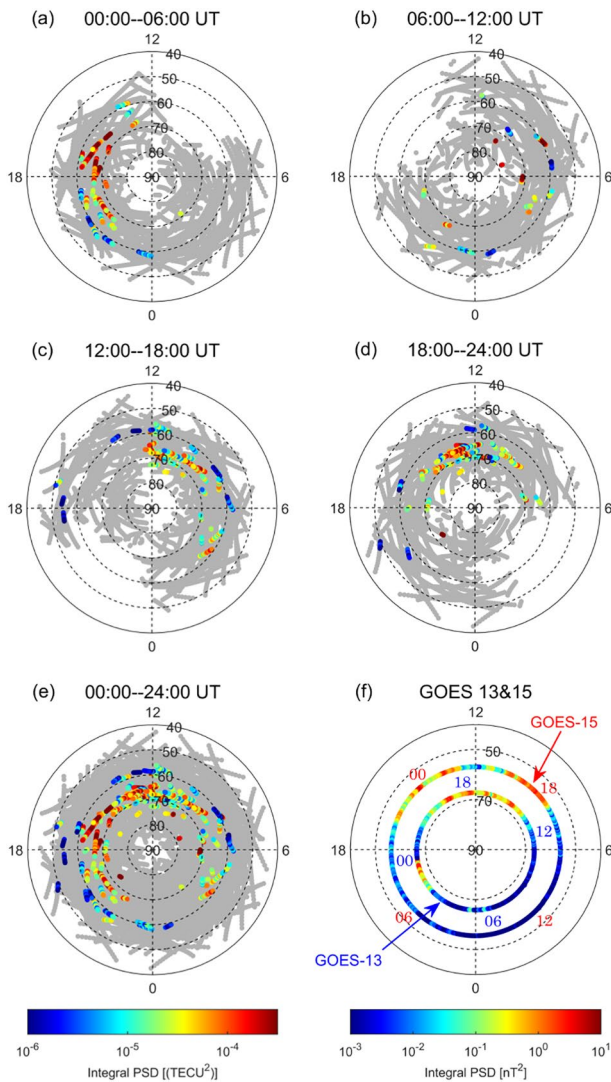


Figure 4. Magnetic latitude and magnetic local time distribution of high-m ultralow frequency (ULF) wave signatures in GPS vertical total electron content (VTEC) and GOES measurements on January 25, 2016. The color scales in (a–f) indicates the integral power spectral density between half maximum frequencies and 5–15 mHz, respectively. (a–d): Time evolution of ULF wave signatures in GPS VTEC data over 4 successive 6-h time intervals. (e and f) Show the ULF wave signatures in GPS VTEC and the GOES satellites B_z component on January 25, 2016 throughout the day.

not surprisingly, we found no clear correlation between the ULF wave occurrence and ionospheric amplitude scintillation.

3.3. Time Evolution of ULF Wave 2D Spatial Distribution

To investigate the temporal evolution and 2D spatial structures of the high-m ULF waves in the ionosphere, VTEC measurements from all 10 GPS receivers (red asterisks) shown in Figure 1e are processed. ULF wave signatures are automatically identified using full width at half maximum (Takahashi & Ukhorskiy, 2007), continuity and standard deviation filters (see Text S2 and Figures S2–S8 in Supporting Information for details). Figure 4 shows the MLAT and MLT distributions of the integrated high-m ULF wave PSD in the VTEC and GOES B_z component on January 25, 2016. Figures 4a–4d show time evolution of ULF wave signatures in GPS VTEC data over 4 successive 6-hour time intervals. The wave signatures appeared near dusk with relatively stronger power but as the GPS receivers rotate with Earth into the nightside, the wave signatures tended to gradually disappear. When the GPS receivers moved into the dayside, the wave signatures were observed again in VTEC observations and they were mainly constrained to local noon. Note that in Figure 4b, ULF wave signatures observed from 06 to 12 UT were significantly reduced compared with the other UT intervals, even with GPS satellite paths covering the morning sector. The IMF variations shown in Figure 1c during this time interval made it difficult to distinguish the narrowband wave signatures from broadband waves and other ionospheric disturbances in GPS VTEC (one example is shown in Figure S5 in Supporting Information).

Figures 4e and 4f show the high-m ULF wave signatures in VTEC as well as GOES-13 and GOES-15 B_z components on January 25, 2016. For visualization purposes, the magnetic latitudes of the GOES-15 footprints were moved 10° equatorward. The blue and red numbers indicate the UTs of the GOES-13 and GOES-15 observations, respectively. Figure 4e shows the ULF waves were visible in the TEC data on the dayside and in the post-dusk sector. The power in the afternoon sector was relatively larger than at other MLTs. Note that there are wave signatures identified around 80° MLAT. These are probably outliers associated with ionospheric disturbances rather than ULF waves driven by drift-bounce resonance (Watson, Jayachandran, & MacDougall, 2016). In Figure 4f, ULF wave signatures from GOES satellites observations occurred mainly on the dayside. Due to the limitations in spatial coverage, GOES-13 measurements started at 00:00 UT of January 25, 2016 from the post dusk sector and did not show the wave signatures around 18:00 MLT. Based on the widely distributed GPS receivers, the VTEC measurements give a more complete 2D spatial distribution as well as the time evolution of the high-m ULF waves than the GOES satellites measurements.

4. Discussion

The MLAT-MLT distribution of ULF waves and its temporal evolution are critical constraints needed for understanding the role of wave-particle interactions in ring current and radiation belt dynamics (Oimatsu et al., 2018; Zong et al., 2009). However, because of the limited high time resolution measurements from coherent and incoherent scatter radars as well as sparse satellite in-situ observations, it is difficult to determine the spatial and temporal distribution of ULF waves in a single event. In this study, by taking advantage of the widely distributed GPS VTEC observations, which cover from ~50° MLAT to near the magnetic pole, we obtained the global high-m ULF wave spatial distribution (Figure 4e) during a single event. In addition,

VTEC observations which cover more than 200° in geomagnetic longitude also provide constraints of the wave distribution in MLT. Using data from 10 GPS receivers we also examined the temporal evolution of the 2D spatial structure of the ULF wave PSD (Figures 4a–4d). For future work, the onset time of this kind of long-lasting ULF wave observed during the recovery phase of geomagnetic storms (Table 1 in Shi, Baker, et al., 2018) can be identified and the 2D spatial distribution of ULF waves during the wave onset can also be obtained using multi-point GPS TEC data. This information can be used to further investigate the driver of ULF waves, which is difficult to obtain using satellite observations alone (Archer et al., 2018). The altitude of the IPP is assumed to be 450 km. It is still unknown at what altitude range the ULF modulation of TEC occurs. The distribution range will expand (decrease) with the increase (decrease) of the assumed IPP altitude.

Shi, Baker, et al. (2018) estimated the m value (−258, westward propagating) of this ULF event using the drift-bounce resonance theory. Watson, Jayachandran, Singer, et al. (2016) also observed high- m mode Pc4 ULF waves in TEC data. By applying a multi-satellite triangulation technique, the m value was estimated to be −240 to −310 and −20 to −40 in the former and latter periods of a 16-minute time interval, respectively. However, these waves were detected by ground magnetometers and GOES satellites with an estimated m value of −35 to −60. This study presents the first GPS TEC observations of high- m ULF waves that were screened by the ionosphere and not detected by ground magnetometers. Note that Pc5 waves were present in GPS TEC (Figures 2g and 2h), ground magnetometer (Figures 2g–2i), and GOES observations (Figure 3a). These are low- m toroidal waves which have been investigated in Shi et al. (2020) and are beyond the scope of this study.

When very high-frequency radio signals pass through plasma irregularities in the ionosphere, random fluctuations will occur in their parameters such as phase, amplitude, and propagating direction. This effect is referred to as ionospheric scintillation (Jiao et al., 2013). In addition to TEC disturbances, ULF waves have also been found to contribute to ionospheric scintillations (Francia et al., 2020; Yizengaw et al., 2018). However, as shown in Figures 3e and 3f, no significant variation in phase sigma index and S4 index (not shown) were observed during the wave activity that occurred during this event, which suggests high- m ULF waves made little contribution to ionospheric scintillation.

Pilipenko et al. (2014) proposed several possible mechanisms for how ULF waves might produce TEC modulation, including periodic particle precipitation, plasma compression by reflected fast mode waves, ion heating, field-aligned plasma transport, etc. The VTEC fluctuations related to high- m ULF waves in this study may be caused by plasma transport in field-aligned current due to Alfvén waves (Pilipenko et al., 2014). The modification of the recombination coefficient induced by ion heating may be also responsible for the VTEC modulations (Baddeley et al., 2017; Kozyreva et al., 2020). Consideration of physical mechanisms for generating ULF wave signatures in TEC data is left to future study.

5. Conclusions

Multi-instrument observations from space and the ground have been used to investigate high- m ULF wave signatures during the recovery phase of the geomagnetic storm that occurred from January 24 to 26, 2016. GPS VTEC data captured ULF wave signatures similar to those seen in GOES B_r data and SuperDARN LOS velocity observations. The high- m poloidal wave perturbations were screened by the ionosphere and not detected by ground magnetometers. WTC and XTW results showed the detrended GPS VTEC data had high coherence and significant common power with the GOES-15 B_r data. The ULF wave signatures in VTEC data showed similar temporal distribution and frequency time evolution to GOES-15 B_r data. By comparing the MLAT and UT distribution of the phase sigma index of FSIC with the ULF wave occurrence, we found the high- m ULF waves during this event made little contribution to ionospheric scintillation. An automatic identification procedure is developed to detect ULF signatures in GPS VTEC data. Based on measurements from 10 GPS receivers on January 25, 2016, the time evolution and 2D spatial structures of high- m ULF waves in the ionosphere were revealed for the first time. The high- m ULF wave signatures in the GPS VTEC data were mainly observed on the dayside and continue into the post dusk sector over MLATS from ~64° to ~71°. The abundance of GPS VTEC measurements is an excellent resource that can be further exploited

to provide new insights into the ionospheric response to ULF waves including their temporal and spatial characteristics.

Data Availability Statement

The GPS data are provided by the Crustal Dynamics Data Information System (CDDIS) (<https://cddis.nasa.gov/>) and Canadian High Arctic Ionospheric Network (CHAIN) (<http://chain.physics.unb.ca/chain/>). The authors acknowledge the use of SuperDARN data. SuperDARN is a collection of radars funded by national scientific funding agencies of Australia, Canada, China, France, Italy, Japan, Norway, South Africa, United Kingdom and the United States of America. We thank the Virginia Tech SuperDARN group for the distribution of SuperDARN data via the website (<http://vt.superdarn.org/tiki-index.php?page=-Data+Access>). The GOES magnetic field data are available from NOAA National Centers for Environmental Information (<https://www.ncei.noaa.gov/>). The FSIM and SNKQ ground magnetometer data are obtained from the CANMOS network (<https://www.nrcan.gc.ca/science-data/research-centres-labs/geological-survey-canada/17100>).

Acknowledgments

Work at Virginia Tech was supported by National Science Foundation (NSF) grant AGS-1935110. M. D. Hartinger was supported by NSF grants PLR-1744828 and AGS-2027210. D. Lin is supported by the Advanced Study Program (ASP) of the National Center for Atmospheric Research (NCAR). NCAR is sponsored by NSF. We would like to thank Mary Hudson for the internal review. We also thank Chris Watson and one anonymous reviewer whose comments and suggestions helped improve this manuscript.

References

- Archer, M. O., Hartinger, M. D., Redmon, R., Angelopoulos, V., Walsh, B. M., & Hill, E. (2018). First results from sonification and exploratory citizen science of magnetospheric ULF waves: Long-lasting decreasing-frequency poloidal field line resonances following geomagnetic storms. *Space Weather*, *16*(11), 1753–1769. <https://doi.org/10.1029/2018SW001988>
- Baddeley, L., Yeoman, T., Wright, D., Trattner, K., & Kellet, B. (2004). A statistical study of unstable particle populations in the global ring current and their relation to the generation of high m ULF waves. *Annales Geophysicae, European Geosciences Union*, *22*(12), 4229–4241. <https://doi.org/10.5194/angeo-22-4229-2004>
- Baddeley, L. J., Lorentzen, D. A., Partamies, N., Denig, M., Pilipenko, V. A., Oksavik, K., et al. (2017). Equatorward propagating auroral arcs driven by ULF wave activity: Multipoint ground- and space-based observations in the dusk sector auroral oval. *Journal of Geophysical Research: Space Physics*, *122*(5), 5591–5605. <https://doi.org/10.1002/2016ja023427>
- Davies, K., & Hartmann, G. (1976). Short-period fluctuations in total columnar electron content. *Journal of Geophysical Research*, *81*(19), 3431–3434. <https://doi.org/10.1029/ja081i019p03431>
- Foufoula-Georgiou, E., & P. Kumar (Eds.). *Wavelets in geophysics*. Elsevier.
- Francia, P., Regi, M., De Lauretis, M., Pezzopane, M., Cesaroni, C., Spogli, L., & Raita, T. (2020). A case study of correspondence between Pc1 activity and ionospheric irregularities at polar latitudes. *Earth Planets and Space*, *72*(1). <https://doi.org/10.1186/s40623-020-01184-4>
- Grinsted, A., Moore, J. C., & Jevrejeva, S. (2004). Application of the cross wavelet transform and wavelet coherence to geophysical time series. *Nonlinear Processes in Geophysics*, *11*(5/6), 561–566. <https://doi.org/10.5194/npg-11-561-2004>
- Hughes, W., & Southwood, D. (1976). The screening of micropulsation signals by the atmosphere and ionosphere. *Journal of Geophysical Research*, *81*(19), 3234–3240. <https://doi.org/10.1029/ja081i019p03234>
- Jacobs, J., Kato, Y., Matsushita, S., & Troitskaya, V. (1964). Classification of geomagnetic micropulsations. *Journal of Geophysical Research*, *69*(1), 180–181. <https://doi.org/10.1029/jz069i001p00180>
- Jiao, Y., Morton, Y. T., Taylor, S., & Pelgrum, W. (2013). Characterization of high-latitude ionospheric scintillation of GPS signals. *Radio Science*, *48*(6), 698–708. <https://doi.org/10.1002/2013rs005259>
- Kozyreva, O. V., Pilipenko, V. A., Bland, E. C., Baddeley, L. J., & Zakharov, V. I. (2020). Periodic modulation of the upper ionosphere by ULF waves as observed simultaneously by SuperDARN radars and GPS/TEC technique. *Journal of Geophysical Research: Space Physics*, *125*, e2020JA028032. <https://doi.org/10.1029/2020ja028032>
- Le, G., Chi, P. J., Strangeway, R. J., Russell, C. T., Slavin, J. A., Takahashi, K., et al. (2017). Global observations of magnetospheric high-m poloidal waves during the 22 June 2015 magnetic storm. *Geophysical Research Letters*, *44*(8), 3456–3464. <https://doi.org/10.1002/2017GL073048>
- Oimatsu, S., Nosé, M., Takahashi, K., Yamamoto, K., Keika, K., Kletzing, C., et al. (2018). Van Allen Probes observations of drift-bounce resonance and energy transfer between energetic ring current protons and poloidal Pc4 wave. *Journal of Geophysical Research: Space Physics*, *123*(5), 3421–3435. <https://doi.org/10.1029/2017ja025087>
- Pilipenko, V., Belakhovsky, V., Murr, D., Fedorov, E., & Engebretson, M. (2014). Modulation of total electron content by ULF Pc5 waves. *Journal of Geophysical Research: Space Physics*, *119*(6), 4358–4369. <https://doi.org/10.1002/2013ja019594>
- Ren, J., Zong, Q., Wang, Y., & Zhou, X. (2015). The interaction between ULF waves and thermal plasma ions at the plasmaspheric boundary layer during substorm activity. *Journal of Geophysical Research: Space Physics*, *120*(2), 1133–1143. <https://doi.org/10.1002/2014ja020766>
- Sarris, T., Wright, A., & Li, X. (2009). Observations and analysis of Alfvén wave phase mixing in the Earth's magnetosphere. *Journal of Geophysical Research*, *114*, A03218. <https://doi.org/10.1029/2008JA013606>
- Shah, A., Waters, C., Sciffer, M., & Menk, F. (2016). Energization of outer radiation belt electrons during storm recovery phase. *Journal of Geophysical Research: Space Physics*, *121*(11), 10845–10860. <https://doi.org/10.1002/2016ja023245>
- Shepherd, S. G. (2014). Altitude-adjusted corrected geomagnetic coordinates: Definition and functional approximations. *Journal of Geophysical Research: Space Physics*, *119*(9), 7501–7521. <https://doi.org/10.1002/2014ja020264>
- Shi, X., Baker, J. B. H., Ruohoniemi, J. M., Hartinger, M. D., Murphy, K. R., Rodriguez, J. V., et al. (2018). Long-lasting poloidal ULF waves observed by multiple satellites and high-latitude SuperDARN radars. *Journal of Geophysical Research: Space Physics*, *123*(10), 8422–8438. <https://doi.org/10.1029/2018JA026003>
- Shi, X., Hartinger, M. D., Baker, J. B. H., Ruohoniemi, J. M., Lin, D., Xu, Z., et al. (2020). Multipoint conjugate observations of day-side ULF waves during an extended period of radial IMF. *Journal of Geophysical Research: Space Physics*, *125*(11), e2020JA028364. <https://doi.org/10.1029/2020ja028364>

- Shi, X., Ruohoniemi, J. M., Baker, J. B. H., Lin, D., Bland, E. C., Hartinger, M. D., & Scales, W. A. (2018). Survey of ionospheric Pc3-5 ULF wave signatures in SuperDARN high time resolution data. *Journal of Geophysical Research: Space Physics*, *123*(5), 4215–4231. <https://doi.org/10.1029/2017JA025033>
- Skone, S. (2009). Using GPS TEC measurements to detect geomagnetic Pc3 pulsations. *Radio Science*, *44*(01), 1–10. <https://doi.org/10.1029/2008rs004106>
- Takahashi, K., Oimatsu, S., Nosé, M., Min, K., Claudepierre, S. G., Chan, A., et al. (2018). Van Allen Probes observations of second harmonic poloidal standing Alfvén waves. *Journal of Geophysical Research: Space Physics*, *123*(1), 611–637. <https://doi.org/10.1002/2017ja024869>
- Takahashi, K., & Ukhorskiy, A. Y. (2007). Solar wind control of Pc5 pulsation power at geosynchronous orbit. *Journal of Geophysical Research: Space Physics*, *112*, A11205. <https://doi.org/10.1029/2007JA012483>
- Watson, C., Jayachandran, P., Singer, H. J., Redmon, R. J., & Danskin, D. (2015). Large-amplitude GPS TEC variations associated with Pc5–6 magnetic field variations observed on the ground and at geosynchronous orbit. *Journal of Geophysical Research: Space Physics*, *120*(9), 7798–7821. <https://doi.org/10.1002/2015ja021517>
- Watson, C., Jayachandran, P. T., & MacDougall, J. W. (2016). Characteristics of GPS TEC variations in the polar cap ionosphere. *Journal of Geophysical Research: Space Physics*, *121*, 4748–4768. <https://doi.org/10.1002/2015JA022275>
- Watson, C., Jayachandran, P. T., Singer, H. J., Redmon, R. J., & Danskin, D. (2016). GPS TEC response to Pc4 “giant pulsations”. *Journal of Geophysical Research: Space Physics*, *121*(2), 1722–1735. <https://doi.org/10.1002/2015ja022253>
- Yizengaw, E., Zesta, E., Moldwin, M., Magoun, M., Tripathi, N., Surussavadee, C., & Bamba, Z. (2018). ULF wave-associated density irregularities and scintillation at the equator. *Geophysical Research Letters*, *45*(11), 5290–5298. <https://doi.org/10.1029/2018GL078163>
- Zong, Q. G., Zhou, X. Z., Li, X., Song, P., Fu, S., Baker, D., et al. (2007). Ultralow frequency modulation of energetic particles in the dayside magnetosphere. *Geophysical Research Letters*, *34*, L12105. <https://doi.org/10.1029/2007GL029915>
- Zong, Q. G., Zhou, X. Z., Wang, Y. F., Li, X., Song, P., Baker, D. N., et al. (2009). Energetic electron response to ULF waves induced by interplanetary shocks in the outer radiation belt. *Journal of Geophysical Research: Space Physics*, *114*(A10), A10204. <https://doi.org/10.1029/2009ja014393>